J. Plasma Phys. (2025), *vol*. 91, E89
 doi:10.1017/S0022377825100391

Nonlinear modulation of arbitrary intense electromagnetic waves in magnetized electron–positron plasmas with temperature

Yuee Luo[1], Xuewen Wang[2], Jianhui Wu[2], Quanshui Zhu[3] and Feng Yang[4]

[1]School of Mechanical and Electronic Engineering, Jingdezhen University, Jingdezhen 333400, PR China
[2]School of Information Engineering, Jingdezhen University, Jingdezhen 333400, PR China
[3]National Demonstration Center for Experimental College Physics Education (NCHU), Nanchang Hangkong University, Nanchang 330063, PR China
[4]School of Mechanical and Electronic Engineering, Jingdezhen Ceramic University, Jingdezhen 333403, PR China

Corresponding author: Xuewen Wang, icewater0397@163.com

(Received 17 January 2025; revision received 29 April 2025; accepted 29 April 2025)

A theoretical framework has been established to investigate the modulational instability of electromagnetic waves in magnetized electron–positron plasmas. The framework is capable of analyzing electromagnetic waves of any intensity and plasmas at any temperature. A fully relativistic hydrodynamic model, incorporating relativistic velocities and thermal effects, is used to describe the relativistic dynamics of particles in plasmas. Under the weakly magnetized approximation, a modified nonlinear Schrödinger equation, governing the dynamics of the envelope of electromagnetic waves in plasmas, is obtained. The growth rate of the modulational instability is then given both theoretically and numerically. By analyzing the dependence of the growth rate on some key physical parameters, the coupled interplay of relativistic effects, ponderomotive forces, thermal effects and magnetic fields on electromagnetic waves can be clarified. The findings demonstrate that specific combinations of physical parameters can significantly enhance modulational instability, providing a theoretical basis for controlling the propagation of electromagnetic waves in plasmas. This framework has broad applicability to most current laser–plasma experiments and high-energy radiation phenomena from stellar surfaces.

Key words: Modulational instability, Electromagnetic waves, Magnetized plasmas, Nonlinear wave equation

1. Introduction

Magnetized electron–positron (EP) plasmas widely exist in many high-energy astrophysical environments, such as accretion disks (Filho 2009), pulsar magnetospheres (Sturrock 1971; Luo & Ji 2012), black holes (Putten & Maurice 1999; Laurent & Titarchuk 2018) and so on. In the pulsar magnetosphere, pair plasma is generated through a cascade process of EP pair production, and becomes highly

magnetized due to the super-strong magnetic field of the pulsar. Additionally, EP plasmas form near black hole horizons during gamma-ray flares emitted by stellar-mass black holes. Therefore, these environments serve as natural laboratories for studying interactions between electromagnetic waves and magnetized EP plasmas.

In recent years, with the rapid development of laser technology, both experimental and theoretical studies have pointed out that an EP plasma can also be generated under laboratory conditions (Sarri *et al*. 2015). In 1997, Burke *et al*. (1997) reported the first laboratory production of positrons by colliding a 46.6 GeV electron beam with a terawatt laser pulse at 527 nm wavelength. Ridgers *et al*. (2012) numerically simulated the pair-production process in which a laser with an intensity of $4 \times 10^{23}\,\mathrm{W\,cm^{-2}}$ strikes an aluminum target, producing an EP plasma with the maximum density of $10^{26}\,\mathrm{cm^{-3}}$. Used the ASTRA-GEMINI laser system (the peak intensity of the laser is $3 \times 10^{19}\,\mathrm{W\,cm^{-2}}$), Sarri *et al*. (2015) achieved an EP plasma density of $10^{16}\,\mathrm{cm^{-3}}$. Li *et al*. (2017) proposed an all-optical scheme for ultra-bright gamma-ray emission and dense positron production with lasers at an intensity of $10^{22-23}\,\mathrm{W\,cm^{-2}}$, in which a positron beam with a density of $2.5 \times 10^{22}\,\mathrm{cm^{-3}}$ was achieved. Gong *et al*. (2020) investigated the momentum spectrum and number density of created EP pairs in frequency-modulated laser fields. These studies provide a window for investigating laboratory astrophysics at laser facilities.

If there exists a magnetic field, we will achieve a magnetized EP plasma in the laboratory. The magnetic source may be an external magnetic field, such as in magnetic confinement fusion experiments where a strong magnetic field is applied to the plasma, or may be a self-generated magnetic field arising from laser–plasma interactions (Lehner 2000; Najmudin *et al*. 2001; Tatarakis *et al*. 2002; Abudurexiti, Okada & Ishikawa 2009). Self-generated magnetic fields can also be generated by a laser-induced plasma in the process of inertial confinement fusion implosion (Srinivasan, Dimonte & Tang 2012; Walsh *et al*. 2017; Sadler *et al*. 2022).

In the previously mentioned high-energy astrophysical environments and intense laser–plasma systems, plasmas typically possess well-defined temperatures. For example, the order of magnitude of the plasma temperature in the pulsar magnetosphere is reported to be $10^6\,\mathrm{K}$ (Helfand, Chanan & Novick 1980; Timokhin & Harding 2019). This kind of plasma is referred to as a cold or warm plasma, in which the thermal energy of a particle is much smaller than its rest energy, that is $k_\mathrm{B}T_j \ll m_j c^2$, with k_B being the Boltzmann constant, the subindex j denoting the species of the particles in the plasma, T_j being the temperature of the j type of particle, m_j being the rest mass of the j type of particle, c being the speed of light in vacuum. An electron temperature in the laser channel was found to be several MeV, which is given by the two-dimensional particle-in-cell (PIC) simulations of the laser channeling in millimeter-scale underdense plasmas for fast ignition (Li *et al*. 2008). A peak plasma temperature as high as 40 MeV was achieved in laser-driven ion acceleration processes, studied via PIC simulations (Weng *et al*. 2016). Such plasmas are termed relativistic hot plasmas due to the condition $k_\mathrm{B}T_j \gg m_j c^2$.

In this paper, we focus on the modulational instability (MI) of intense electromagnetic waves in a magnetized EP plasma, which is one of the fundamental phenomena in the nonlinear interaction between electromagnetic waves and plasmas (Shukla, Marklund & Eliasson 2004; Sprangle, Hafizi & Peñano 2020). Nonlinear development of the MI plays a key role in many nonlinear processes, such as envelope solitons, envelope shocks, freak waves and self-focusing of electromagnetic waves (Jha *et al*. 2006; Lehmann, Laedke & Spatschek 2008; Abedi-Varaki & Jafari 2017; Roozehdar Mogaddam *et al*. 2018; Das, Chandra & Ghosh 2020; Cheng *et al*. 2023).

https://doi.org/10.1017/S0022377825100391 Published online by Cambridge University Press

Spurred by the significance of MI in electromagnetic waves, researchers have extensively studied this phenomenon under different kinds of physical conditions over the past few decades (Shukla & Bharuthram 1987; Chen, Liu & Li, 2011; Sprangle, Esarey & Hafizi 1997; Rozina *et al*. 2016; Luo & Wang 2020). Some studies have specifically addressed MI in magnetized plasmas. For instance, the MI of laser pulses in transversely magnetized underdense plasmas is investigated by Jha *et al*. (2005), analyzing magnetic field effects. The MI of the right-hand elliptically polarized laser pulses in cold magnetized EP plasmas is explored by Chen *et al*. (2011). While the MI of circularly polarized electromagnetic waves and the formation of the solitary waves in hot magnetized EP plasmas are studied by Asenjo *et al*. (2012). The MI of intense lasers in hot magnetized EP plasmas in the quasi-neutral limit is examined by Sepehri Javan (2012), discussing the dependences of the MI on the plasma temperature and external magnetic fields. Sobacchi *et al*. (2021) investigated self-modulation of fast radio bursts in pulsars, analyzing instabilities developing for arbitrary directions of the perturbation wave vector. However, these researchers primarily focus on the propagation of electromagnetic waves with normalized amplitude $a_0 < 1$ (corresponding to laser intensities $I < 10^{18}\mathrm{W/cm^2}$) in low-temperature plasmas where $k_\mathrm{B}T_j < m_j c^2$. To date, the MI of electromagnetic waves with arbitrary intensity in relativistic hot plasmas is rarely discussed. This paper addresses this gap by studying MI across intensities ranging from weakly relativistic ($a_0 \ll 1$) to ultra-relativistic ($a_0 \gg 1$) regimes in magnetized EP plasmas. For this purpose, we employ a fully relativistic fluid model (Asenjo *et al*. 2009), incorporating a temperature-dependent function to characterize plasma thermal effects.

The paper is structured as follows. In § 2, a nonlinear wave equation is obtained under the weak magnetization approximation, which characterizes the amplitude evolution of electromagnetic waves in magnetized EP plasmas. In § 3, the growth rate of MI is derived. In § 4, through numerical analysis in both low-temperature and high-temperature regimes, we examined the dependence of the MI growth rate on some key physical parameters. Furthermore MI characteristics of γ-rays emitted by a pulsar are investigated. Finally, the principal findings are summarized in § 5.

2. Nonlinear wave equations

In the following, the propagation of an electromagnetic wave in a magnetized EP plasma is investigated. The plasma system maintains local equilibrium with charge neutrality, expressed as $n_{e0} = n_{p0}$, where n_{e0} and n_{p0} are unperturbed densities of electrons and positrons in the laboratory frame. A circularly polarized electromagnetic wave is considered to propagate along the external magnetic field $\boldsymbol{B}_0 = B_0\hat{\boldsymbol{e}}_z$. The corresponding vector potential $\boldsymbol{A}$ of the laser can be expressed as

$$\boldsymbol{A} = \tfrac{1}{2}A(z,t)(\hat{\boldsymbol{e}}_x + i\sigma\hat{\boldsymbol{e}}_y)\exp[i(k_0 z - \omega_0 t)] + c.c., \tag{2.1}$$

where ω_0 is the frequency of the wave, k_0 is the wavenumber, $\sigma = +1$ (-1) denotes the right-hand (left-hand) circularly polarized wave and $A(z,t)$ is the slowly varying amplitude satisfying the condition

$$\left|\frac{1}{\omega_0}\frac{\partial A}{\partial t}\right| \ll |A|. \tag{2.2}$$

https://doi.org/10.1017/S0022377825100391 Published online by Cambridge University Press

From the Maxwell equations and using

$$\boldsymbol{E} = -\frac{1}{c}\frac{\partial \boldsymbol{A}}{\partial t} - \nabla\phi,\ \boldsymbol{B} = \nabla \times \boldsymbol{A} + \boldsymbol{B}_0, \tag{2.3}$$

we can obtain the wave equation

$$\frac{1}{c^2}\frac{\partial^2 \boldsymbol{A}}{\partial t^2} - \nabla^2 \boldsymbol{A} = \frac{4\pi}{c}\boldsymbol{J}, \tag{2.4}$$

where $\boldsymbol{J} = \sum_j -\eta_j e n_j \boldsymbol{p}_j/(\gamma_j m)$ is the current density of the pair plasma, e is the charge of an electron or a positron, $j = e$, p denote the electron and positron, respectively, $\eta_e = 1$ and $\eta_p = -1$ are charge polarity indicators, m is the rest mass of an electron or a positron and n_j, $\boldsymbol{p}_j$ and $\gamma_j = [1 + p_j^2/(m^2c^2)]^{1/2}$ are the number density, momentum and Lorentz factor of j sort of particles, respectively.

The relativistic fluid momentum equation for the j type of plasma particle can be represented as (Asenjo *et al*. 2012)

$$\left(\frac{\partial}{\partial t} + \frac{\boldsymbol{p}_j}{\gamma_j m}\cdot\nabla\right)(f_j \boldsymbol{p}_j) = \eta_j\left[\frac{e}{c}\frac{\partial \boldsymbol{A}}{\partial t} + e\nabla\phi - \frac{e}{\gamma_j mc}\boldsymbol{p}_j \times (\nabla \times \boldsymbol{A}) - \frac{\omega_c}{\gamma_j}\boldsymbol{p}_j \times \boldsymbol{e}_z\right] - \frac{1}{n_j}\nabla \Pi_j, \tag{2.5}$$

where the pressure of particles $\Pi_j = n_j k_{\mathrm{B}} T_j$ for an ideal gas, $\omega_c = eB_0/(mc)$ is the electron cyclotron frequency, and ϕ is the scalar potential satisfying Poisson's equation

$$\nabla^2\phi = 4\pi e(n_e - n_p). \tag{2.6}$$

In the equation (2.5), f_j is a function of temperature. It can be expressed as $f_j = K_3(mc^2/k_{\mathrm{B}}T_j)/K_2(mc^2/k_{\mathrm{B}}T_j)$, assuming that the plasma system follows a relativistic Maxwell–Jüttner distribution, where $K_3(x)$ and $K_2(x)$ are modified Bessel functions of order 3 and 2 (Asenjo *et al*. 2012; Banerjee, Dutta & Misra 2020). The function can be approximated by $f_j \approx 1 + 5k_{\mathrm{B}}T_j/(2\,\mathrm{mc}^2)$ in the low-temperature limit $k_{\mathrm{B}}T_j \ll mc^2$, while $f_j \approx 4k_{\mathrm{B}}T_j/(mc^2)$ in the high-temperature limit $k_{\mathrm{B}}T_j \gg mc^2$.

By substituting equation (2.1) into (2.5), we can obtain the momentum of plasma particles from the high-frequency response of moving particles to the incident wave

$$\boldsymbol{p}_j = \eta_j \frac{mc\boldsymbol{a}}{f_j - \eta_j \frac{\sigma\mu}{\gamma_j}}, \tag{2.7}$$

where $\mu = \omega_c/\omega_0$ is the normalized cyclotron frequency, and $\boldsymbol{a} = e\boldsymbol{A}/(mc^2)$ is the normalized vector potential.

Substituting the expression (2.7) into $\gamma_j = [1 + p_j^2/(m^2c^2)]^{1/2}$, we can derive

$$\gamma_j^2 - 1 = \frac{a^2}{\left(f_j - \eta_j \frac{\sigma\mu}{\gamma_j}\right)^2}. \tag{2.8}$$

For weakly magnetized plasmas, the condition $\mu \ll f_j\gamma_j$ holds. In this limit, the right-hand side of the (2.8) can be expanded as a power series in μ. Retaining terms

https://doi.org/10.1017/S0022377825100391 Published online by Cambridge University Press

to first order in μ, the equation for the Lorentz factors simplifies to

$$\gamma_j^3 - \left(1 + \frac{a^2}{f_j^2}\right)\gamma_j - \eta_j \frac{2a^2\sigma\mu}{f_j^3} = 0. \tag{2.9}$$

Thus the approximate solutions for the Lorentz factors of each fluid can be expressed as

$$\gamma_j \approx \left(1 + \frac{a^2}{f_j^2}\right)^{\frac{1}{2}} + \eta_j \frac{a^2\sigma\mu}{f_j^3\left(1 + \frac{a^2}{f_j^2}\right)}. \tag{2.10}$$

From equation (2.5), we can also obtain the equation that the plasma density perturbation satisfies

$$k_{\mathrm{B}} T_j \nabla \ln n_j = \nabla\left(\eta_j e\phi - \varphi_{pj}\right), \tag{2.11}$$

where φ_{pj} is the relativistic ponderomotive potential, expressed as

$$\varphi_{pj} = mc^2\left(f_j\gamma_j + \eta_j \frac{\sigma\mu}{2}\ln\gamma_j - \eta_j \frac{\sigma\mu}{4\gamma_j^2}\right). \tag{2.12}$$

In the absence of an external magnetic field, the ponderomotive potential reduces to the standard expression in a cold plasma $\varphi_{pj} = mc^2\gamma_j$. By integrating equation (2.11), and assuming the plasma being unperturbed at infinity, i.e. using the boundary conditions $n_{e,p} = n_{e0,p0}$, $\phi \to 0$ and $\gamma \to 1$ at $|z| \to \infty$, we can obtain the number densities of electrons and positrons

$$n_j = n_{j0}\exp\left\{\beta_j\left[\eta_j\Phi - f_j(\gamma_j - 1) - \eta_j\frac{\sigma\mu}{2}\ln\gamma_j - \eta_j\frac{\sigma\mu}{4}\left(1 - \frac{1}{\gamma_j^2}\right)\right]\right\}, \tag{2.13}$$

where $\Phi = e\phi/(mc^2)$, $\beta_j = mc^2/(k_{\mathrm{B}}T_j)$.

Substituting (2.13) into the quasi-neutrality condition $n_e - n_p - n_{i0} = 0$, we obtain

$$\begin{aligned}(\beta_p + \beta_e)\Phi = {} & \beta_p\left[f_p(1 - \gamma_p) + \frac{\sigma\mu}{2}\ln\gamma_p + \frac{\sigma\mu}{4}\left(1 - \frac{1}{\gamma_p^2}\right)\right] \\ & - \beta_e\left[f_e(1 - \gamma_e) - \frac{\sigma\mu}{2}\ln\gamma_e - \frac{\sigma\mu}{4}\left(1 - \frac{1}{\gamma_e^2}\right)\right].\end{aligned} \tag{2.14}$$

Substituting the expression of Φ into (2.13), and assuming the plasma to be in thermal equilibrium, i.e. $f_e = f_p = f$, the number density of the j-particle can be rewritten as

$$n_j = n_{j0}\exp\{\beta\xi(\gamma_e, \gamma_p)\}, \tag{2.15}$$

where $\beta = 2\beta_e\beta_p/(\beta_p + \beta_e)$ is the temperature parameter, the function

$$\xi(\gamma_e, \gamma_p) = \left[f(1 - \bar{\gamma}) + \frac{\sigma\mu}{4}\ln\frac{\gamma_p}{\gamma_e} + \frac{\sigma\mu}{8}\left(\frac{1}{\gamma_e^2} - \frac{1}{\gamma_p^2}\right)\right], \tag{2.16}$$

and $\bar{\gamma} = (\gamma_e + \gamma_p)/2$.

https://doi.org/10.1017/S0022377825100391 Published online by Cambridge University Press

Substituting the vector potential $\boldsymbol{A}$ and current density $\boldsymbol{J}$ into (2.4) yields the electromagnetic-wave envelope equation

$$c^2\frac{\partial^2 a}{\partial z^2}-\frac{\partial^2 a}{\partial t^2}+i2\left(\omega_0\frac{\partial a}{\partial t}+k_0c^2\frac{\partial a}{\partial z}\right)+\left(\omega_0^2-k_0^2c^2\right)a=\frac{4\pi e^2}{m}\left(\frac{n_p}{f\gamma_p+\sigma\mu}+\frac{n_e}{f\gamma_e-\sigma\mu}\right)a. \tag{2.17}$$

Linearizing equation (2.17), we can get the nonlinear dispersion relation of the wave

$$\omega_0^2-k_0^2c^2=Q_L\omega_{pe}^2, \tag{2.18}$$

where $\omega_{pe}=(4\pi e^2n_{e0}/m)^{1/2}$ is the plasma frequency in the laboratory frame, and

$$Q_L=\left(\frac{1}{f+\sigma\mu}+\frac{1}{f-\sigma\mu}\right). \tag{2.19}$$

The dispersion relationship can also be expressed in a more common form

$$\omega_0^2-k_0^2c^2=\frac{2f\omega_0^2\omega_{pe}^2}{f^2\omega_0^2-\omega_c^2}. \tag{2.20}$$

For $f=1$, the dispersion relation for a cold plasma is recovered. Let $k_0=0$, the cutoff frequency of the electromagnetic wave in the magnetized pair plasma can be obtained as

$$\omega_{\text{cut}}=\sqrt{\frac{\omega_c^2}{f}+2\omega_{pe}^2}. \tag{2.21}$$

Obviously, the cutoff frequency of waves decreases with the increasing of the plasma temperature in the hot plasmas.

Substituting equations (2.15) and (2.18) into equation (2.17), leads to

$$\frac{1}{2}\left(c^2\frac{\partial^2 a}{\partial z^2}-\frac{\partial^2 a}{\partial t^2}\right)+i\left(\omega_0\frac{\partial a}{\partial t}+k_0c^2\frac{\partial a}{\partial z}\right)+D_{NL}\omega_{pe}^2a=0, \tag{2.22}$$

where $D_{NL}=\{Q_L-Q\exp[\beta\xi(\gamma_e,\gamma_p)]\}/2$ and

$$Q=\left(\frac{1}{f\gamma_p+\sigma\mu}+\frac{1}{f\gamma_e-\sigma\mu}\right). \tag{2.23}$$

Introducing the dimensionless variables $\tau=\omega_{pe}^2t/\omega_0$, $\tilde{z}=\omega_{pe}z/c+u_g\tau$, $u_g=(\omega_0/\omega_{pe})v_g/c$, where $v_g=kc^2/\omega_0$ is the group velocity of the wave, we write (2.22) as

$$\frac{1}{2}\frac{\partial^2 a}{\partial\tilde{z}^2}+i\frac{\partial a}{\partial\tau}+D_{NL}a=0, \tag{2.24}$$

where the slowly varying envelope approximation is used. Equation (2.24) is the modified nonlinear Schrödinger equation governing the dynamics of the envelope of an electromagnetic wave in magnetized EP plasmas.

https://doi.org/10.1017/S0022377825100391 Published online by Cambridge University Press

The theoretical framework is derived under the weakly magnetized approximation, requiring the magnetic field strength to satisfy $\omega_c \ll f_j\gamma_j\omega_0$. This condition remains broadly applicable to most contemporary laser–plasma experiments and high-energy radiation processes on stellar surfaces.

For instance, in experiments utilizing magnetic fields of the order of $10^4 - 10^5$ G, such as those in magnetic confinement fusion research, the weak magnetization condition is trivially met. Modern solid-state and conventional electromagnets can generate fields up to 10^6 G (Sims *et al*. 2008), corresponding to electron cyclotron frequencies of $\omega_c \sim 10^{13}\ \mathrm{s}^{-1}$. To satisfy $\omega_c \ll f_j\gamma_j\omega_0$ in such systems, laser wavelengths below 10 μm ($\omega_0 > 10^{14}\ \mathrm{s}^{-1}$) are typically sufficient. In scenarios involving stronger fields, such as inertial confinement fusion experiments with $10^6 - 10^7$ G fields ($\omega_c \sim 10^{13} - 10^{14}\ \mathrm{s}^{-1}$), near-infrared lasers (e.g. Nd lasers at 1.06 μm, $\omega_0 = 1.8 \times 10^{15}\ \mathrm{s}^{-1}$) still comply with the approximation. This robustness extends to ultra-intense laser–plasma interactions generating several kilo-tesla fields (Knauer *et al*. 2010; Fujioka *et al*. 2013), where $\omega_c \sim 10^{15}\ \mathrm{s}^{-1}$. Here, even mid-infrared lasers (3–10 μm) remain viable due to the relativistic and thermal effects ($f_j\gamma_j \gg 1$). Recently, some studies have proposed laser-driven schemes to generate ultra-strong magnetic fields of the order of 10^8 G (corresponding to $\omega_c \sim 10^{15}\ \mathrm{s}^{-1}$) (Wilson *et al*. 2021; Shi *et al*. 2023). For such fields, in cold and weakly relativistic plasmas ($f_j\gamma_j \approx 1$), the laser frequency must far exceed $10^{15}\ \mathrm{s}^{-1}$. If ultraviolet or X-ray lasers ($\omega_0 \geq 10^{16}\ \mathrm{s}^{-1}$) are used, the model remains applicable. While relativistic hot plasmas ($f_j\gamma_j \gg 1$) significantly relax this constraint. The weak magnetization condition still holds even for laser frequencies below $10^{15}\ \mathrm{s}^{-1}$.

This framework also accommodates astrophysical environments like pulsar surfaces, where typical magnetic fields reach 10^{12} G ($\omega_c \sim 10^{19}\ \mathrm{s}^{-1}$). For such systems, the weak magnetization condition demands radiation frequencies exceeding $10^{19}\ \mathrm{s}^{-1}$, naturally aligning with X-ray or γ-ray emission processes.

3. Modulational instability

The MI of electromagnetic waves can be analyzed using a common method introduced in references (Shukla & Bharuthram 1987; Shukla *et al*. 2004). Assume that

$$a = (a_0 + a_1)e^{i\delta\tau}, \tag{3.1}$$

where a_0 is a real constant, $a_1 (\ll a_0)$ denotes the small perturbation amplitude and δ represents the nonlinear frequency shift. Substituting (3.1) into (2.24), and linearizing the resulting equation with respect to a_1, we obtain the nonlinear frequency shift at the lowest order

$$\delta = D_{NL}(|a| = a_0), \tag{3.2}$$

where $D_{NL}(|a| = a_0) = [Q_L - Q_0 e^{\beta\xi(\gamma_{e0},\gamma_{p0})}]/2$, $Q_0 = 1/(f\gamma_{p0} + \sigma\mu) + 1/(f\gamma_{e0} - \sigma\mu)$ and $\gamma_{j0} = \gamma_j(|a| = a_0)$.

By analyzing the first-order terms in the derived equation, we obtain an equation governing the perturbation amplitude

$$\frac{1}{2}\frac{\partial^2 a_1}{\partial\tilde{z}^2} + i\frac{\partial a_1}{\partial\tau} + \Lambda a_0^2(a_1 + a_1^*) = 0, \tag{3.3}$$

https://doi.org/10.1017/S0022377825100391 Published online by Cambridge University Press

where

$$\Lambda = \frac{1}{4}\exp[\beta\xi(\gamma_{e0},\gamma_{p0})]\left[\frac{f\Gamma_p}{(f\gamma_{p0}+\sigma\mu)^2}+\frac{f\Gamma_e}{(f\gamma_{e0}-\sigma\mu)^2}-\beta Q_0(s_e\Gamma_e+s_p\Gamma_p)\right], \tag{3.4}$$

$$s_j = -\frac{f}{2}+\eta_j\frac{\sigma\mu}{4}\left(\frac{1}{\gamma_{j0}}-\frac{1}{\gamma_{j0}^3}\right), \tag{3.5}$$

and

$$\Gamma_j = \frac{1}{f^2\left(1+a_0^2/f^2\right)^{1/2}}+\eta_j\frac{2\sigma\mu}{f^3}\left[\frac{1}{\left(1+a_0^2/f^2\right)^{1/2}}-\frac{a_0^2}{f^2\left(1+a_0^2/f^2\right)^2}\right]. \tag{3.6}$$

Inserting $a_1 = X + \mathrm{i}Y$ into (3.3) yields

$$\frac{1}{2}\frac{\partial^2 X}{\partial\tilde{z}^2}-\frac{\partial Y}{\partial\tau}+2\Lambda a_0^2 X = 0, \tag{3.7}$$

and

$$\frac{1}{2}\frac{\partial^2 Y}{\partial\tilde{z}^2}+\frac{\partial X}{\partial\tau} = 0. \tag{3.8}$$

For the real part X and imaginary part Y of a_1, we consider the following oscillation forms: $X = \tilde{X}\exp(iK\tilde{z}-i\Omega\tau)$ and $Y = \tilde{Y}\exp(iK\tilde{z}-i\Omega\tau)$, where $\tilde{X}$ and $\tilde{Y}$ are the real amplitudes, K is the modulation wavenumber normalized by ω_{pe}/c and Ω is the modulation frequency normalized by ω_{pe}^2/ω_0. The nonlinear dispersion relation of MI is obtained as

$$\Omega^2 = -\frac{K^2}{2}\left[2\Lambda a_0^2-\frac{K^2}{2}\right], \tag{3.9}$$

from which we can extract the MI growth rate $\Gamma = -i\Omega$ as follows:

$$\Gamma = \frac{K}{\sqrt{2}}\left(2\Lambda a_0^2-\frac{K^2}{2}\right)^{\frac{1}{2}}. \tag{3.10}$$

We can see that the result degenerates to the growth rate formula of Shukla *et al.* (Shukla *et al.* 2004), for the cold non-magnetized pair plasmas.

When $K = (2\Lambda)^{1/2}a_0$ that is the modulation wavenumber of the fastest-growing mode, the growth rate of MI has a maximum

$$\Gamma_{\max} = \Lambda a_0^2. \tag{3.11}$$

As can be seen from the previous derivation process, the MI of the electromagnetic field in the magnetized plasmas is closely related to the coupling effect of the ponderomotive force, thermal pressure, relativistic effect and magnetic field.

4. Numerical results and discussions

In this section, we numerically analyze factors influencing the growth rate of MI, with a focus on two plasma regimes: the low-temperature limit ($\beta_j \gg 1$) and high-temperature limit ($\beta_j \ll 1$). Owing to the symmetry of the EP plasma, the modes of the circularly polarized electromagnetic waves do not affect its MI. Therefore, we set $\sigma = 1$ in the numerical calculations presented below.

https://doi.org/10.1017/S0022377825100391 Published online by Cambridge University Press

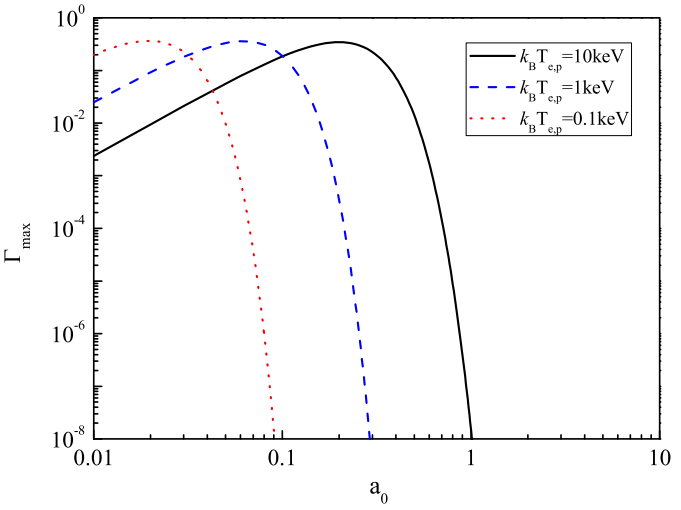

FIGURE 1. The variations of the function $\Gamma_{\max}$ with the electromagnetic-wave amplitude a_0 for different particle temperatures $k_{\mathrm{B}}T_{e,p}$ in the low-temperature limit, with fixed parameter $\mu = 0.1$.

4.1. *Numerical analysis*

4.1.1. In the low-temperature limit

For the case of the low-temperature limit, $k_{\mathrm{B}}T_j \ll mc^2 \approx 510$ keV ($\beta_j \gg 1$). The dependence of the maximum growth rate of MI ($\Gamma_{\max}$) on the amplitude of electromagnetic wave a_0 is shown in figure 1, where the particle temperatures $k_{\mathrm{B}}T_{e,p}$ are 0.1, 1 and 10 keV, respectively. It can be seen that, initially, the maximum growth rate gradually increases with an increase in the amplitude of electromagnetic wave for a fixed particle temperature. When the amplitude of the electromagnetic wave increases to a critical value (threshold), the maximum growth rate reaches its peak (maximum value), and then begins to decrease. This behavior can be attributed to the competition between the ponderomotive force of the electromagnetic wave and relativistic effects. As the intensity of the electromagnetic wave increases, the ponderomotive force also increases, causing more particles to be pushed out of their original regions and thereby enhancing the disturbance acting on the electromagnetic wave. However, when the amplitude of the electromagnetic wave increases further, the mass of the particle becomes larger, and the relativistic effect gradually takes over. This makes it increasingly difficult for the ponderomotive force to displace the particles.

The maximum growth rate $\Gamma_{\max}$ as a function of the particle temperature $k_{\mathrm{B}}T_{e,p}$ for different amplitudes of electromagnetic wave $a_0 = 0.01, 0.1, 0.5$ is shown in figure 2. For a fixed amplitude a_0, with the increase of temperature, the function $\Gamma_{\max}$ initially increases and then decreases. As the temperature rises, the thermal pressure increases significantly. It should be noted that the ponderomotive force also increases, as indicated by the exponential term $\exp\{\beta\xi(\gamma_{e0}, \gamma_{p0})\}$ in the expression of $\Gamma_{\max}$. At low temperatures, the ponderomotive force exceeds the thermal pressure and dominates, leading to an enhancement of MI. The growth rate reaches its maximum when these two forces balance each other. However, as the temperature continues to increases, the thermal pressure becomes dominant, resulting in a suppression of MI.

https://doi.org/10.1017/S0022377825100391 Published online by Cambridge University Press

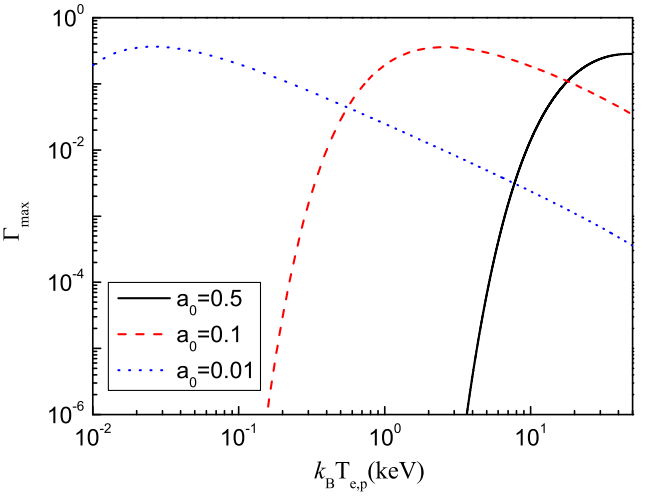

FIGURE 2. The variations of the function $\Gamma_{\max}$ with the particle temperature $k_B T_{e,p}$ in the low-temperature limit for different electromagnetic-wave amplitudes a_0, with fixed parameter $\mu = 0.1$.

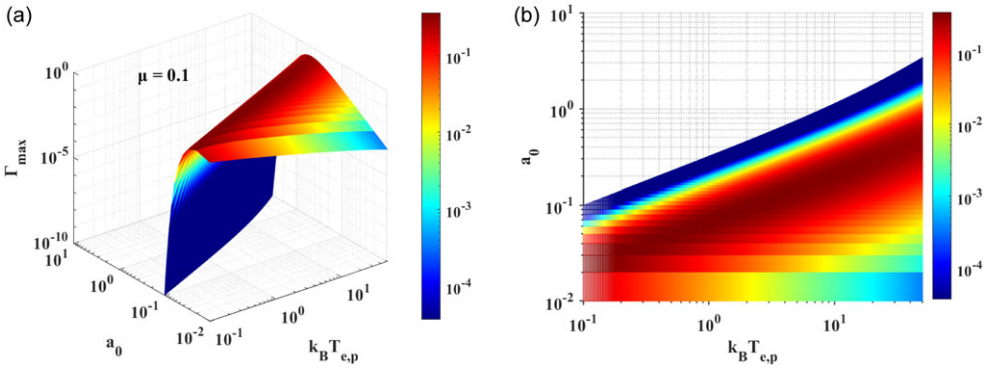

FIGURE 3. Low-temperature limit ($\mu = 0.1$): (*a*) dependence of $\Gamma_{\max}$ on a_0 and $k_B T_{e,p}$, (*b*) phase diagram of MI in the a_0-$k_B T_{e,p}$ plane.

In order to give the law of the growth rate of MI with the amplitude of electromagnetic waves a_0 and particle temperature $k_B T_{e,p}$ more clearly, we plot the results in figure 3. Figure 3(*a*) presents a three-dimensional plot of the maximum growth rate $\Gamma_{\max}$ versus a_0 and $k_B T_{e,p}$ under low-temperature conditions, where a_0 ranges from 0.01 to 10, and $k_B T_{e,p}$ spans 0.1 to 50 keV. Figure 3(*b*) displays the MI phase diagram in the a_0-$k_B T_{e,p}$ parameter space. These figures clearly reveal the combinations of physical parameters associated with higher instability, providing insights for controlling electromagnetic-wave propagation in plasmas.

Figure 4 depicts the dependence of the maximum growth rate $\Gamma_{\max}$ on the magnetic parameter μ under low-temperature conditions. The dependence of the growth rate on the magnetic field is governed by the electromagnetic-wave intensity a_0 and plasma temperature $k_B T_{e,p}$. For example, at $a_0 = 0.1$ and $k_B T_{e,p} = 1$ keV, $\Gamma_{\max}$ exhibits a monotonic decrease with increasing magnetic field. Conversely, at $a_0 = 0.1$

https://doi.org/10.1017/S0022377825100391 Published online by Cambridge University Press

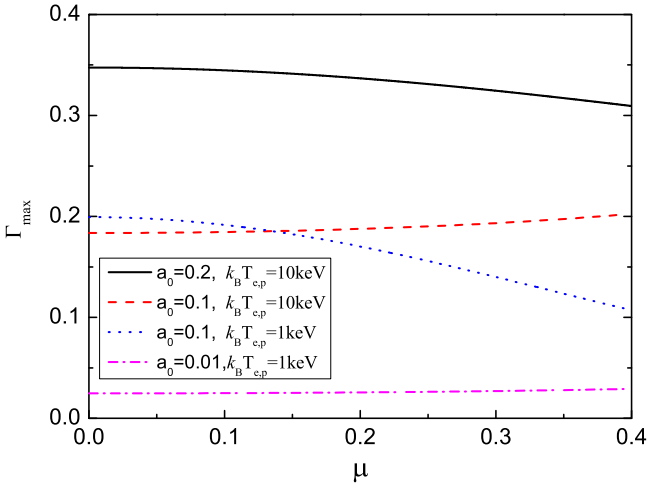

FIGURE 4. The variations of the function $\Gamma_{\max}$ with the magnetic parameter μ for different electromagnetic-wave amplitudes a_0 and particle temperatures $k_{\mathrm{B}}T_{e,p}$ in low-temperature limit.

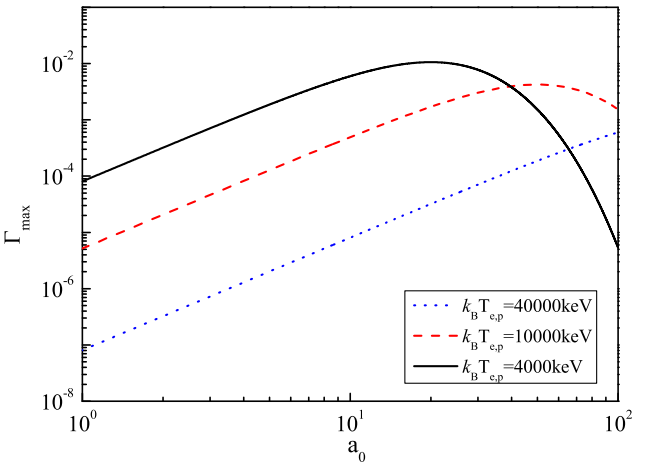

FIGURE 5. The variations of the function $\Gamma_{\max}$ with the electromagnetic-wave amplitude a_0 for different particle temperatures $k_{\mathrm{B}}T_{e,p}$ in the high-temperature limit, with fixed parameter $\mu = 0.1$.

and $k_{\mathrm{B}}T_{e,p} = 10$ keV, $\Gamma_{\max}$ increases gradually with the increasing of the magnetic field. Furthermore, for fixed temperatures ($k_{\mathrm{B}}T_{e,p} = 1$ or 10 keV), at low intensities ($a_0 = 0.01$ or 0.1), enhancing the magnetic field elevates $\Gamma_{\max}$, while at high intensities ($a_0 = 0.1$ or 0.2), the trend reverses. These observations align with the predictions in Sepehri Javan (2012), which focused on weakly relativistic and low-temperature regimes.

4.1.2. In the high-temperature limit

Figures 5–8 demonstrate the growth rate of MI versus the amplitude of electromagnetic waves a_0, particle temperatures $k_{\mathrm{B}}T_{e,p}$ and magnetic field strength in the high-temperature limit $k_{\mathrm{B}}T_j \gg mc^2 \approx 510$ keV ($\beta_j \ll 1$). A comparison between

https://doi.org/10.1017/S0022377825100391 Published online by Cambridge University Press

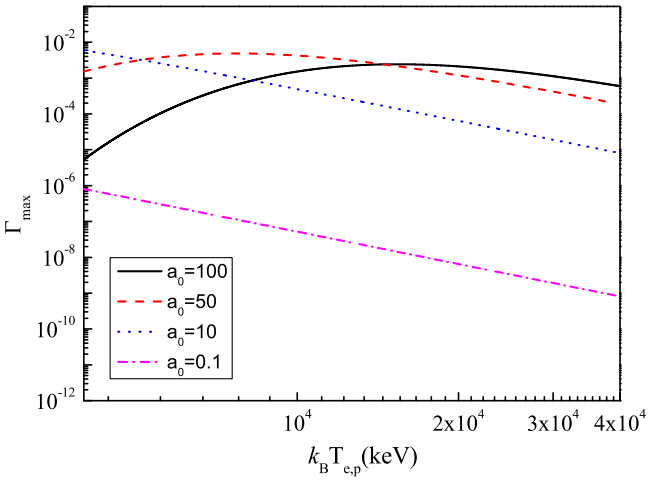

FIGURE 6. The variations of the function $\Gamma_{\max}$ with the particle temperature $k_B T_{e,p}$ in the low-temperature limit for the different electromagnetic-wave amplitudes a_0, with fixed parameter $\mu = 0.1$.

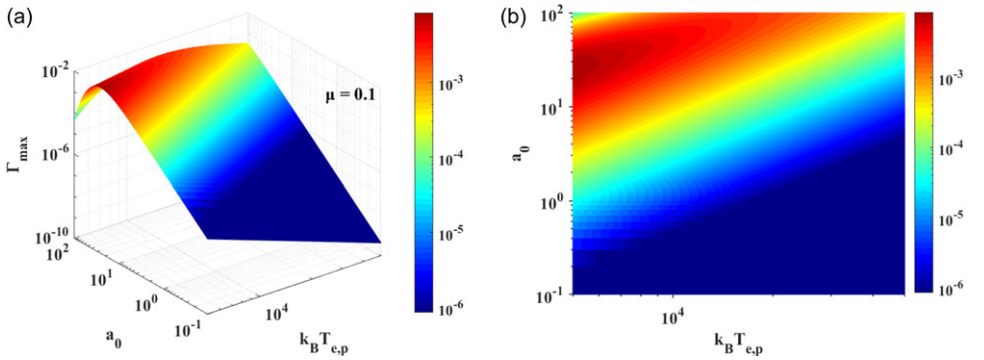

FIGURE 7. High-temperature limit ($\mu = 0.1$): (*a*) dependence of $\Gamma_{\max}$ on a_0 and $k_B T_{e,p}$, (*b*) phase diagram of MI in the a_0-$k_B T_{e,p}$ plane.

figures 1 and 5 reveals that the growth rate of MI increases firstly and then decreases with rising a_0, while the value of a_0 corresponding to the maximum value of the curve becomes larger.

Figure 6 shows the behavior of the function $\Gamma_{\max}$ with the particle temperatures, where relativistic-temperature plasma exhibits stronger modulation efficiency on high-intensity electromagnetic waves. The corresponding three-dimensional plot and the phase diagram in the a_0-$k_B T_{e,p}$ plane are given in figure 7, where a_0 ranges from 0.1 to 100, and $k_B T_{e,p}$ ranges from 5 to 50 MeV. The analysis reveals a suppression of MI growth rate for low-intensity waves ($a_0 < 1$) in relativistic hot plasmas, whereas high-intensity waves ($a_0 > 1$) experience enhanced modulation.

The dependence of the function $\Gamma_{\max}$ on the magnetic parameter μ in the limit of high temperature is shown in figure 8. The figure demonstrates that variations in magnetic field strength exhibit negligible influence on the MI of the

https://doi.org/10.1017/S0022377825100391 Published online by Cambridge University Press

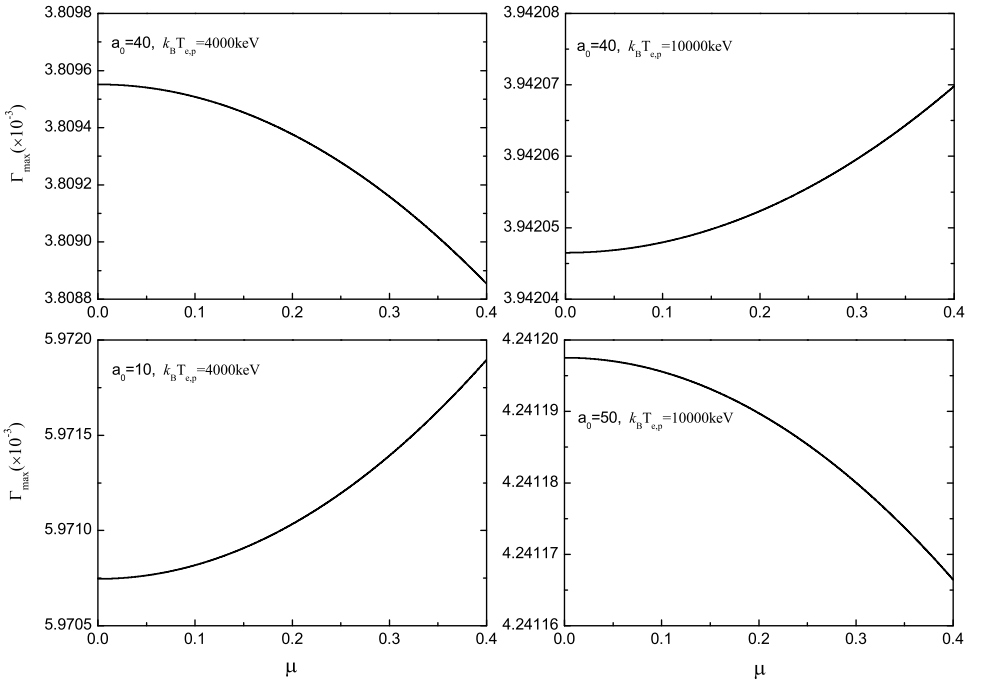

FIGURE 8. The variation of the function $\Gamma_{\max}$ with the magnetic parameter μ for different amplitudes of electromagnetic waves a_0 and particle temperatures $k_{\mathrm{B}}T_{e,p}$ in the high-temperature limit.

electromagnetic wave under high-temperature plasma conditions. For example, at $a_0 = 40$ and $k_{\mathrm{B}}T_{e,p} = 4000$ keV, $\Gamma_{\max}$ decreases marginally from 3.80955×10^{-3} to 3.80885×10^{-3} as the parameter μ increases from 0 to 0.4, corresponding to a relative reduction of 0.018 %.

4.2. *Examples: MI of high-energy radiation in pulsar*

In the following, we investigate the MI of the γ-ray radiation emitted from the pulsar as it propagates through the magnetized pair plasmas. Here, we consider a typical pulsar with an intense intrinsic magnetic fields $B_{\mathrm{s}} \approx 10^{12}$ G at the pulsar surface, a rotation period $P_* \approx 1$ s and a radius $R_* \approx 10$ km. In the polar cap regions, the pair plasma (with the density $n_0 \approx 10^{14} - 10^{16}\,\mathrm{cm}^{-3}$ (Daugherty & Harding 1982)), is produced via cascade processes of EP pairs, from which high-energy radiation is emitted. The pair plasma typically forms behind a thin layer termed the 'pair formation front', located at an altitude $h \approx 10^4$ cm from the star's surface. After generation, the plasma moves outward at high velocity, and may propagate to altitudes of up to $100R_*$.

The plasma temperature in the pulsar magnetosphere is reported to be 10^6 K (Helfand *et al*. 1980), corresponding to $k_{\mathrm{B}}T_{e,p} = 0.1$ keV. The amplitude of the electric field E_0 (in the laboratory frame) produced by the high-energy radiation can be estimated from the luminosity of pulsars as

$$L = \int \boldsymbol{S} \cdot \mathrm{d}\sigma \simeq \frac{cE_0^2}{4\pi} A_{\mathrm{s}}, \tag{4.1}$$

https://doi.org/10.1017/S0022377825100391 Published online by Cambridge University Press

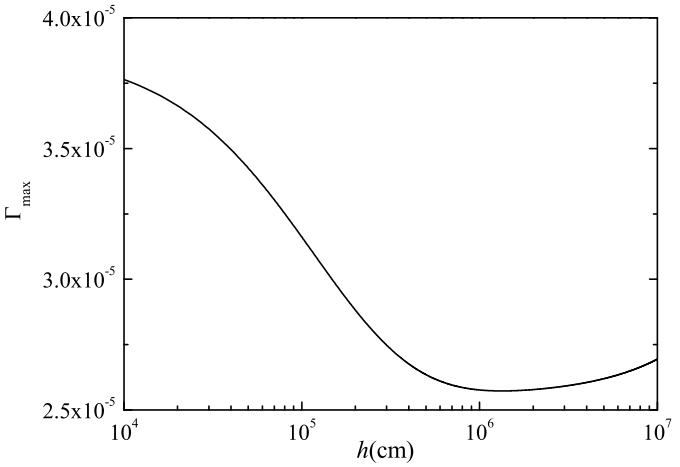

FIGURE 9. The variation of the function $\Gamma_{\max}$ with the altitude h for $a_0 = 10^{-4}$ and $n_0 \approx 10^{16}\,\mathrm{cm}^{-3}$.

where $\boldsymbol{S}$ is the Poynting vector describing the electromagnetic (EM) energy flux, and A_s is the transverse area though which the energy flux flows. Therefore we have

$$E_0 \simeq \sqrt{\frac{4\pi L}{cA_p}}\left(\frac{R_*}{R_* + h}\right), \tag{4.2}$$

where A_p is the polar cap area (with radius $r_p = 10^4 P_*^{-1/2}$ cm), and h is the altitude from the stellar surface. In polar gap models, high-energy emissions originate at lower altitudes $h \approx 10^{-2} R_* = 10^4$ cm (Ruderman & Sutherland 1975; Hibschman 2002). Strong radiation in the bands of γ-rays with luminosity $L_\gamma \approx 10^{33} - 10^{36}$erg/s has been observed from a few pulsars (Ulmer 1994). Therefore, the amplitude of the electric field $E_0 \approx 10^7 - 10^9$esu for γ-rays is estimated. Correspondingly, the normalized vector potential is $a_0 = eE_0/(m_e c\omega_0) \approx 10^{-6} - 10^{-4}$ for γ-rays with $\omega_0 \approx 10^{20}\,\mathrm{s}^{-1}$.

The local magnetic field follows the dipolar approximation

$$B_0 \simeq B_s\left(\frac{R_*}{R_* + h}\right)^3. \tag{4.3}$$

Figure 9 shows the dependence of $\Gamma_{\max}$ on altitude h for $a_0 = 10^{-4}$ and $n_0 \approx 10^{16}\,\mathrm{cm}^{-3}$ (corresponding to $\omega_{pe} = 5.64 \times 10^{12}\,\mathrm{s}^{-1}$), as γ-rays propagate from $h \approx 10^4$ to $h \approx 10^7$ cm. The curve showed a trend of decreasing firstly and then increasing, which is caused by changes in the strength of the magnetic field and the amplitude of the electromagnetic wave.

Using the dimensional growth rate $\Gamma'_{\max} = \Gamma_{\max}\omega_{pe}^2/\omega_0$, the amplitude of electromagnetic radiations being modulated can be written as

$$a = a_0 \exp\left(\int_0^t \Gamma'_{\max}\mathrm{d}t\right). \tag{4.4}$$

The relative amplitude increase $[(a - a_0)/a_0]\,\%$ with the altitude h is shown in figure 10. It shows that the amplitude of the electromagnetic radiation increases

https://doi.org/10.1017/S0022377825100391 Published online by Cambridge University Press

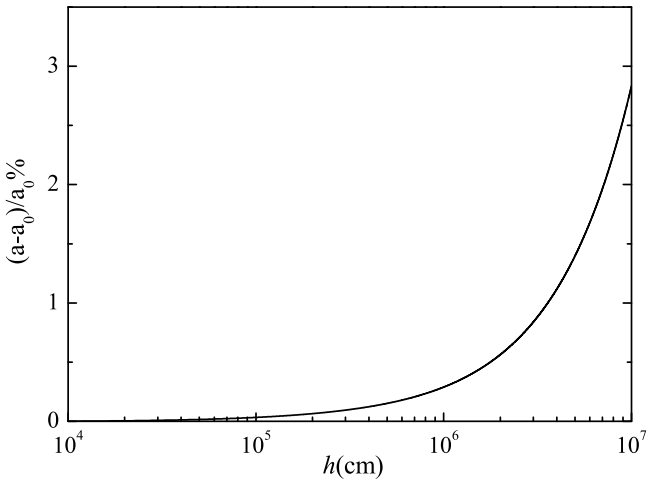

FIGURE 10. The relative amplitude increase $[(a - a_0)/a_0]\,\%$ with the altitude h for $a_0 = 10^{-4}$.

by 2.81 %, when it travels from 10^4 to 10^7 cm in the magnetosphere of the pair plasma.

5. Summary and conclusion

In this work, the MI of an electromagnetic wave propagating along an external magnetic field in an EP plasma is investigated. The normalized amplitude of electromagnetic waves a_0 considered in this work ranges from 0.01 to 100, covering regimes from weakly relativistic to ultra-relativistic. A fully relativistic fluid model for particles is used, in which a temperature-dependent function $f_j = K_3(mc^2/k_\mathrm{B}T_j)/K_2(mc^2/k_\mathrm{B}T_j)$ is included to account for thermal effects. In the regime of weakly magnetized plasmas, we derive a modified nonlinear Schrödinger equation that describes the evolution of the envelope of an electromagnetic wave in magnetized EP plasmas. The dispersion relation and the growth rate of MI are studied theoretically and numerically. The variation of the MI growth rate with the wave amplitude a_0, particle temperature $k_\mathrm{B}T_{e,p}$ and magnetic field strength is analyzed in detail for two limiting cases: the low-temperature limit ($k_\mathrm{B}T_j \ll mc^2$) and the high-temperature limit ($k_\mathrm{B}T_j \gg mc^2$).

Due to the coupled multi-parameter effects, the MI exhibits a non-monotonic dependence on the individual parameters. From the numerical analysis, we draw the following conclusions:

i. When the plasma temperature and magnetic field intensity are fixed, the growth rate of MI increases first and then decreases with increasing wave amplitude.

ii. When the wave amplitude and magnetic field intensity are fixed, the growth rate of MI also demonstrates a non-monotonic trend, initially increasing then decreasing with rising plasma temperature.

iii. At fixed plasma temperature, the growth rate of MI increases with external magnetic field strength for low-intensity waves but decreases for high-intensity waves.

https://doi.org/10.1017/S0022377825100391 Published online by Cambridge University Press

iv. At fixed wave amplitude, the MI growth rate decreases with increasing magnetic field strength for lower plasma temperatures, whereas it increases for higher temperatures. It should be pointed out that the magnetic field-induced variation in growth rate becomes negligible in the high-temperature limit.

We apply the theoretical results obtained in this paper to analyze the MI of gamma rays emitted from the pulsar surface. The result shows that the amplitude of the radiation increases by 2.81 % when propagating from 10^4 to 10^7 cm in the magnetosphere of the pulsar. This study enhances our understanding of the nonlinear dynamics in electromagnetic radiation propagating through magnetized pair plasmas on pulsar surfaces, and provides insights into intense laser–plasma interactions in magnetized hot pair plasmas.

Acknowledgements

Editor Luís O. Silva thanks the referees for their advice in evaluating this article.

Funding

This work is supported by the Project of Jingdezhen University (Grant No. 2022xjkt-02); the Open Fund of the National Demonstration Center for Experimental College Physics Education (NCHU) (Grant No. SY2304); the Science and Technology Planning Project of Jingdezhen City (Grant No. 20161GYZD001-16) and the Science and Technology Project of Provincial Education Department of Jiangxi Province (Grant No. GJJ202816).

Declaration of interests

The authors report no conflict of interest.

REFERENCES

ABEDI-VARAKI, M. & JAFARI, S. 2017 Nonlinear interaction of intense left-and right-hand polarized laser pulse with hotmagnetized plasma. *J. Plasma Phys.* **83** (4), 655830401.

ABUDUREXITI, A., OKADA, T. & ISHIKAWA, S. 2009 A mechanism for self-generated magnetic fields in the interaction of ultra-intense laser pulses with thin plasma targets. *J. Plasma Phys.* **75** (1), 91–98.

ASENJO, F.A., BOROTTO, F.A., CHIAN, A.C.L., MUÑOZ, V., ALEJANDRO VALDIVIA, J. & REMPEL, E.L. 2012 Self-modulation of nonlinear waves in a weakly magnetized relativistic electron-positron plasma with temperature. *Phys. Rev. E* **85** (4), 046406.

ASENJO, F.A., MUÑOZ, V., ALEJANDRO VALDIVIA, J. & HADA, T. 2009 Circularly polarized wave propagation in magnetofluid dynamics for relativistic electron-positron plasmas. *Phys. Plasmas* **16** (12), 122108.

BANERJEE, G., DUTTA, S. & MISRA, A.P. 2020 Large amplitude electromagnetic solitons in a fully relativistic magnetized electron-positron-pair plasma. *Adv. Space Res.* **66** (9), 2265–2273.

BURKE, D.L., *et al.* 1997 Positron production in multiphoton light-by-light scattering. *Phys. Rev. Lett.* **79** (9), 1626–1629.

CHEN, H.Y., LIU, S.Q. & LI, X.Q. 2011 Modulation instability by intense laser beam in magnetized plasma. *Optik* **122** (7), 599–603.

CHENG, Z.M., DENG, D.C., YU, M.Y. & WU, H.C. 2023 Relativistic toroidal light solitons in plasma. *Plasma Sci. Technol.* **25** (3), 032001.

DAS, C., CHANDRA, S. & GHOSH, B. 2020 Amplitude modulation and soliton formation of an intense laser beam interacting with dense quantum plasma: symbolic simulation analysis. *Contrib. Plasma Phys.* **60** (8), e202000028.

DAUGHERTY, J.K. & HARDING, A.K. 1982 Electromagnetic cascades in pulsars. *Astrophys. J.* **252**, 337–347.

FILHO, C.M. 2009 On the double natured solutions to the two-temperature external soft photon comptonized accretion disks. *Astrophys. J.* **700** (2), 1086–1096.

FUJIOKA, S., *et al.* 2013 Kilotesla magnetic field due to a capacitor-coil target driven by high power laser. *Sci. Rep.* **3** (1), 1170.

GONG, C., LI, Z.L., XIE, B.S. & LI, Y.J. 2020 Electron-positron pair production in frequency modulated laser fields. *Phys. Rev. D* **101** (1), 016008.

HELFAND, D.J., CHANAN, G.A. & NOVICK, R. 1980 Thermal X-ray emission from neutron stars. *Nature* **283** (5745), 337–343.

HIBSCHMAN, J.A. 2002 Gamma-ray emission from rotation-powered pulsars. *Astrophys. J.* **565** (2), 1183–1190.

JHA, P., KUMAR, P., RAJ, G. & UPADHYAYA, A.K. 2005 Modulation instability of laser pulse in magnetized plasma. *Phys. Plasmas* **12** (12), 123104.

JHA, P., MISHRA, R.K., UPADHYAYA, A.K. & RAJ, G. 2006 Self-focusing of intense laser beam in magnetized plasma. *Phys. Plasmas* **13** (10), 103102.

KNAUER, J.P., *et al.* 2010 Compressing magnetic fields with high-energy lasers. *Phys. Plasmas* **17** (5), 056318.

LAURENT, P. & TITARCHUK, L. 2018 Electron-positron pair creation close to a black hole horizon: red-shifted annihilation line in the emergent X-ray spectra of a black hole. I. *Astrophys. J.* **859** (2), 89.

LEHMANN, G., LAEDKE, E.W. & SPATSCHEK, K.H. 2008 Two-dimensional dynamics of relativistic solitons in cold plasmas. *Phys. Plasmas* **15** (7), 072307.

LEHNER, T. 2000 Intense self-generated magnetic field in the interaction of a femtosecond laser pulse with an underdense plasma. *Europhys. Lett.* **50** (4), 480–486.

LI, G., YAN, R., REN, C., WANG, T.L., TONGE, J. & MORI, W.B. 2008 Laser channeling in millimeter-scale underdense plasmas of fast-ignition targets. *Phys. Rev. Lett.* **100** (12), 125002.

LI, H.Z., *et al.* 2017 Ultra-bright γ-ray emission and dense positron production from two laser-driven colliding foils. *Sci. Rep.* **7** (1), 17312.

LUO, Y. & JI, P. 2012 Pair production induced by quantum electrodynamic vacuum polarization in pulsar. *Mon. Not. R. Astron. Soc.* **420** (2), 1673–1683.

LUO, Y.E. & WANG, X.W. 2020 Modulational instability of ultraintense laser pulses in electron-positron-ion plasmas including vacuum polarization effect. *Plasma Phys. Control. Fusion* **62** (6), 065004.

NAJMUDIN, Z., TATARAKIS, M., PUKHOV, A., CLARK, E.L., CLARKE, R.J., DANGOR, A.E., FAURE, J., MALKA, V., NEELY, D. & SANTALA, M.I.K. 2001 Measurements of the inverse Faraday effect from relativistic laser interactions with an underdense plasma. *Phys. Rev. Lett.* **87** (21), 215004.

PUTTEN, V. & MAURICE, H.P.M. 1999 Electron-positron outflow from black holes. *Phys. Rev. Lett.* **84** (17), 3752–3755.

RIDGERS, C.P., BRADY, C.S., DUCLOUS, R., KIRK, J.G., BENNETT, K., ARBER, T.D., ROBINSON, A.P.L. & BELL, A.R. 2012 Dense electron-positron plasmas and ultra-intense bursts of gamma-rays from laser-irradiated solids. *Phys. Rev. Lett.* **108** (16), 165006.

ROOZEHDAR MOGADDAM, R., SEPEHRI JAVAN, N., JAVIDAN, K. & MOHAMMADZADEH, H. 2018 Perturbative approach to the self-focusing of intense X-ray laser beam propagating in thermal quantum plasma. *Phys. Plasmas* **25** (11), 112104.

ROZINA, C., TSINTSADE, N.L., MARYAM, N. & KOMAL, S. 2016 Modulation and filamentation instability of ultrarelativistic electromagnetic waves in electron-positron-ion plasma. *Phys. Plasmas* **23** (11), 112303.

RUDERMAN, M.A. & SUTHERLAND, P.G. 1975 Theory of pulsars-polar caps, sparks, and coherent microwave radiation. *Astrophys. J.* **196**, 51–72.

SADLER, J.D., WALSH, C.A., ZHOU, Y. & LI, H. 2022 Role of self-generated magnetic fields in the inertial fusion ignition threshold. *Phys. Plasmas* **29** (7), 072701.

SARRI, G., *et al.* 2015 Generation of neutral and high-density electron-positron pair plasmas in the laboratory. *Nat. Commun.* **6** (1), 6747.

https://doi.org/10.1017/S0022377825100391 Published online by Cambridge University Press

SARRI, G., DIECKMANN, M.E., KOURAKIS, I., PIAZZA, A.D. & ZEPF, M. 2015 Overview of laser-driven generation of electron-positron beams. *J. Plasma Phys.* **81** (4), 455810401.

SEPEHRI JAVAN, N. 2012 Modulation instability of an intense laser beam in the hot magnetized electron-positron plasma in the quasi-neutral limit. *Phys. Plasmas* **19** (12), 122107.

SHI, Y., AREFIEV, A., HAO, J.X. & ZHENG, J. 2023 Efficient generation of axial magnetic field by multiple laser beams with twisted pointing directions. *Phys. Rev. Lett.* **130** (15), 155101.

SHUKLA, P.K. & BHARUTHRAM, R. 1987 Modulational instability of strong electromagnetic waves in plasmas. *Phys. Rev. A* **35** (11), 4889–4891.

SHUKLA, P.K., MARKLUND, M. & ELIASSON, B. 2004 Nonlinear dynamics of intense laser pulses in a pair plasma. *Phys. Lett. A* **324** (2-3), 193–197.

SIMS, J.R., RICKEL, D.G., SWENSON, C.A., SCHILLIG, J.B. & AMMERMAN, C.N. 2008 Assembly, commissioning and operation of the NHMFL 100 Tesla multi-pulse magnet system. *IEEE Trans.Appl. Supercond.* **18** (2), 587–591.

SOBACCHI, E., LYUBARSKY, Y., BELOBORODOV, A.M. & SIRONI, L. 2021 Self-modulation of fast radio bursts. *Mon. Not. R. Astron. Soc.* **500** (1), 272–281.

SPRANGLE, P., ESAREY, E. & HAFIZI, B. 1997 Intense laser pulse propagation and stability in partially stripped plasmas. *Phys. Rev. Lett.* **79** (6), 1046–1049.

SPRANGLE, P., HAFIZI, B. & PEÑANO, J.R. 2000 Laser pulse modulation instabilities in plasma channels. *Phys. Rev. E* **61** (4), 4381–4393.

SRINIVASAN, B., DIMONTE, G. & TANG, X.Z. 2012 Magnetic field generation in Rayleigh-Taylor unstable inertial confinement fusion plasmas. *Phys. Rev. Lett.* **108** (16), 165002.

STURROCK, P.A. 1971 A model of pulsars. *Astrophys. J.* **164**, 529–556.

TATARAKIS, M., GOPAL, A., WATTS, I., BEG, F.N., DANGOR, A.E., KRUSHELNICK, K., WAGNER, U., NORREYS, P.A., CLARK, E.L. & ZEPF, M. 2002 Measurements of ultrastrong magnetic fields during relativistic laser-plasma interactions. *Phys. Plasmas* **9** (5), 2244–2250.

TIMOKHIN, A.N. & HARDING, A.K. 2019 On the maximum pair multiplicity of pulsar cascades. *Astrophys. J.* **871** (1), 12.

ULMER, M.P. 1994 Gamma-ray observations of pulsars. *Astrophys. J. Suppl.* **90**, 789–795.

WALSH, C.A., CHITTENDEN, J.P., MCGLINCHEY, K. & NIASSE, N.P.L. 2017 Self-generated magnetic fields in the stagnation phase of indirect-drive implosions on the national ignition facility. *Phys. Rev. Lett.* **118** (15), 155001.

WENG, S.M., LIU, M., SHENG, Z.M., MURAKAMI, M., CHEN, M., YU, L.L. & ZHANG, J. 2016 Dense blocks of energetic ions driven by multi-petawatt lasers. *Sci. Rep.* **6** (1), 22150.

WILSON, T.C., SHENG, Z.M., ELIASSON, B. & MCKENNA, P. 2021 Magnetic field amplification by high power lasers inunderdense plasma. *Plasma Phys. Control. Fusion* **63** (8), 084001.